

## Research Paper

**Cite this article:** Gupta A, Kansal A, Chawla P (2021). Design of a wearable MIMO antenna deployed with an inverted U-shaped ground stub for diversity performance enhancement. *International Journal of Microwave and Wireless Technologies* **13**, 76–86. <https://doi.org/10.1017/S1759078720000471>

Received: 22 November 2019  
Revised: 7 April 2020  
Accepted: 8 April 2020  
First published online: 19 May 2020


### Key words:

MIMO; open-end slotting; U-shaped ground stub; wearable; broadside radiation

### Author for correspondence:

Anupma Gupta, E-mail: [anupmagupta31@gmail.com](mailto:anupmagupta31@gmail.com)

# Design of a wearable MIMO antenna deployed with an inverted U-shaped ground stub for diversity performance enhancement

Anupma Gupta<sup>1</sup> , Ankush Kansal<sup>1</sup> and Paras Chawla<sup>2</sup>

<sup>1</sup>Department of Electronics and Communication Engineering, Thapar Institute of Engineering and Technology, Patiala, Punjab, India and <sup>2</sup>Department of Electronics and Communication Engineering, University Institute of Engineering, Chandigarh University, Chandigarh, India

## Abstract

A compact multiple input multiple output (MIMO) antenna operating at 2.45 GHz industrial scientific and medical band is presented for wearable devices. Open-end slotting is used to miniaturize the antenna dimensions. Inverted U-shaped ground stub is incorporated to reduce mutual coupling. On-body performance is analyzed on a three-layered equivalent tissue phantom model. The wide bandwidth of 300 MHz and port isolation of 30 dB are obtained from measured results. The antenna shows the efficiency of 40% and directivity of 4.56 dBi when placed at a gap of “s” = 4 mm from the body. Broadside radiation pattern and low specific absorption rate make the antenna suitable for on-body communication. Further, diversity performance is measured in terms of envelope correlation coefficient (ECC), diversity gain (DG), and channel capacity loss (CCL). The value of ECC is 0.025, DG is 9.98 dB, and CCL is 0.12 bits/s/Hz at 2.45 GHz. Antenna robustness is examined by bending the structure at different radii along the x-axis and y-axis. Performance of the proposed structure is reliable with structural deformation.

## Introduction

In recent years, on-body health monitoring devices have attained great popularity. The ongoing miniaturization of sensors has enabled the future healthcare module to integrate into wearable devices. Wide range of applications has been incorporated with wearable devices in the field of proactive health monitoring, training of military/sports person, personal security, and personal computing. Physiological parameters, such as glucose level, blood pressure, temperature, are continuously measured from the human body. Measured information is synchronized with a PC or mobile phones for monitoring and storing [1]. Therefore, the antenna is one of the most important parts of the healthcare modules for ensuring satisfactory power transfer from on-body wearable device to off-body monitoring device.

Several design challenges arise while designing the on-body antenna. Near-field electromagnetic radiations interact with multi-layered tissue structure (consisting of skin, fat, muscle, and bone) and produce internal reflection and scattering. It interrupts with impedance matching and degrades antenna performance [2]. To overcome this issue, various design techniques have been used including cavity-backed surface-integrated waveguide [3, 4], meandered dipole with a reflector ground [5], electromagnetic band gap structure [6], antenna with artificial magnetic conductor [7], and multi-stacked patch [8]. These techniques provide good isolation between the antenna and the human body but have larger and complex geometry which make them difficult to integrate with wearable devices. Higher mode circular patch antennas with shorting pins [9], reconfigurable circular patch [10], and PIFA structure [11] have smaller dimensions; can be considered as a good candidate for wearable devices; however, they have an undesired larger height. Wide bandwidth is also the one major necessity to ensure stable performance when the antenna is placed on different human being [12]. A significant shift in the resonating band has been observed due to structural deformation in [13]. Maximum SAR limit also restricts the radiated power of the antenna. Besides this, multipath fading occurs due to different body postures and movements. Therefore, to enhance the quality of the signal transmission of wearable devices, multiple input multiple output (MIMO) antennas are attaining much attention by researchers. Very few literatures are available for wearable MIMO antenna structures. Dual-band textile MIMO antenna [14], ultra-wide band (UWB) MIMO antenna with a decoupling structure [15], and neutralization line-based UWB MIMO antenna [16] for wearable device have been investigated but [14–16] are designed using textile materials, possess large footprints, and their performance is also affected due to wrinkling, crumpling, and environmental effects. Ground radiation-based loop antenna with two inductive radiators [17], circular co-radiator antenna with high impedance surface [18], and four-element octagonal ring-shaped MIMO [19] are designed for wearable MIMO devices. Authors have used a rigid FR-4 substrate which is not comfortable for the user to wear, and SAR is also not evaluated in [17]. Large

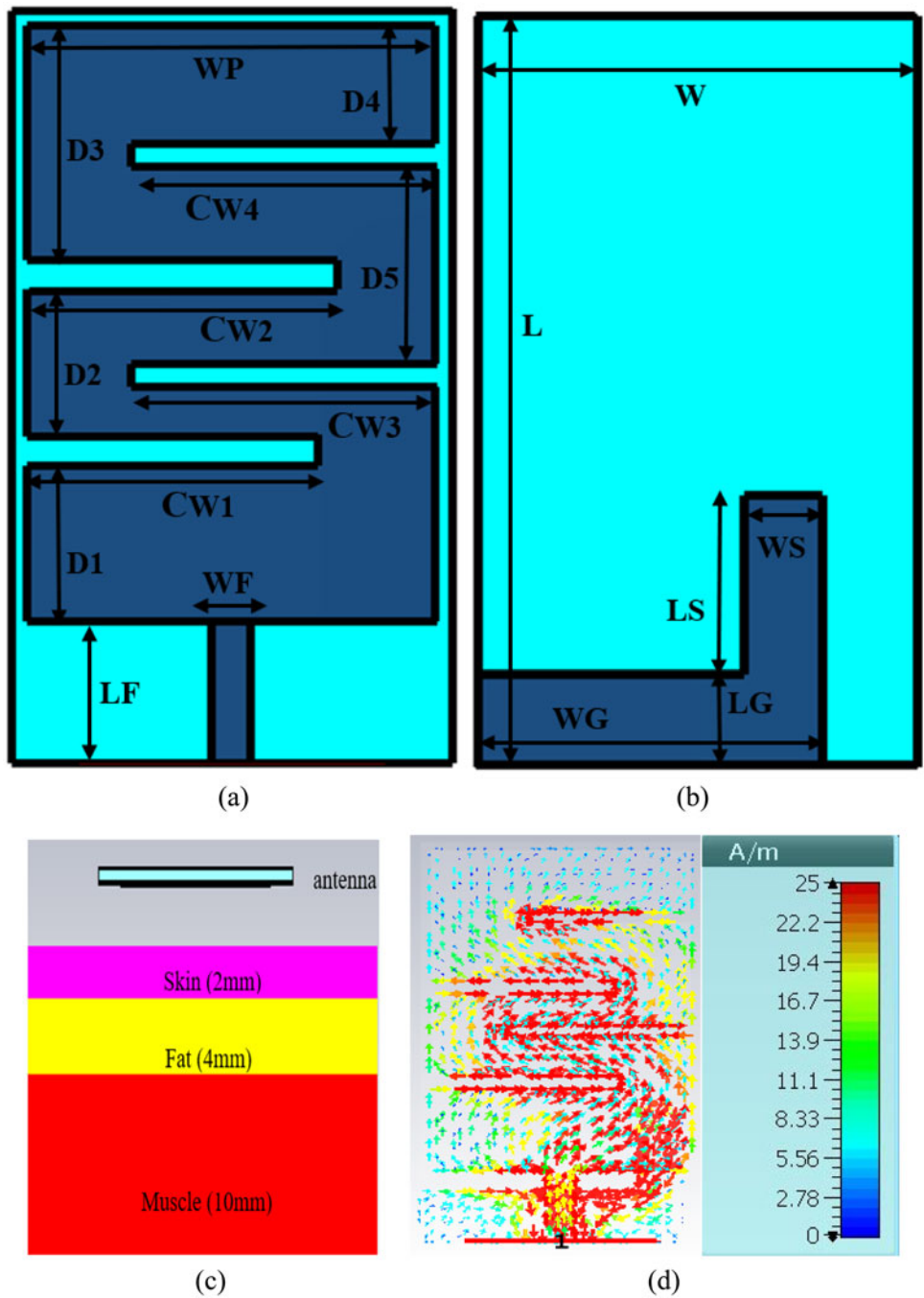


**Fig. 1.** Structure of single-element antenna with simulation setup and surface current distribution: (a) top view, (b) bottom view, (c) simulation setup, (d) surface current.

separation gap between antenna elements is used by researchers to enhance the port isolation which unnecessarily increases the overall size of the MIMO structure.

In this paper, a compact, open-end slotted MIMO antenna structure has been proposed for wearable devices operating at 2.45 GHz (industrial scientific and medical (ISM)) band. First antenna size is miniaturized so that it can be easily integrated with compact on-body devices. After that, a wide bandwidth of 300 MHz is achieved with the help of modified L-shaped ground that makes the antenna robust to withstand frequency detuning. Finally, two antenna elements are used to design the MIMO

structure for enhancing the signal transmission quality. Inverted U-shaped stub is deployed at the ground plane to improve port isolation. Depending on the application of proposed antenna, stringent approaches such as miniaturization, wide operating bandwidth, high port isolation, high directivity, and low specific absorption rate are accomplished by the proposed antenna structure.

**Antenna design procedure**

The antenna is designed on a thin semi-flexible substrate of Rogers 5880 ( $\epsilon_r = 2.2$ , loss  $\tan = 0.0009$ ) with a thickness of

**Fig. 2.** Stepwise structure of single-element antenna: (a) step 1 front view, (b) step 2 front view, (c) step 3 and step 4 front view, (d) back view for step 1–step 3, and (e) step 4 back view.

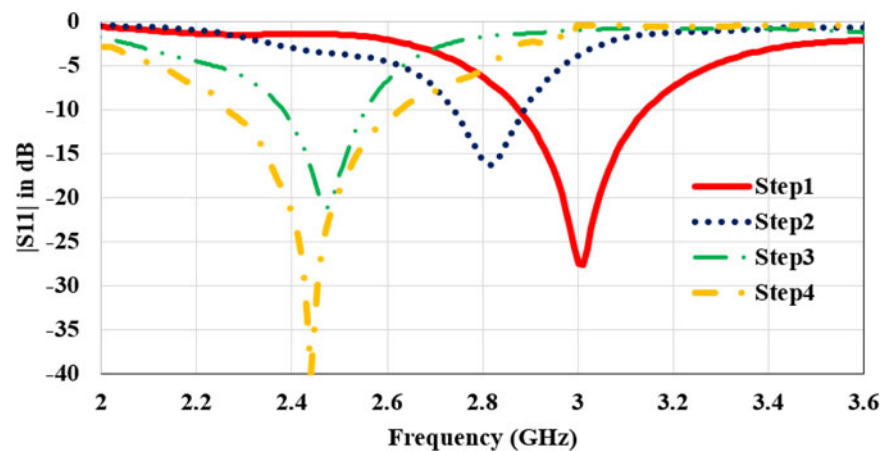
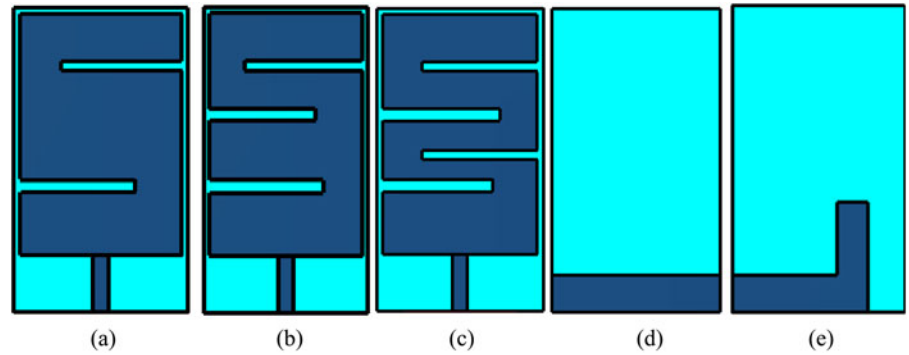


**Fig. 3.** Reflection coefficient of single-element antenna design steps.

0.51 mm. The dimensions of single-element antenna structure are only  $14 \text{ mm} \times 25 \text{ mm}$  that is equal to  $0.114\lambda_0 \times 0.204\lambda_0$ , where  $\lambda_0$  is the free space wavelength at the resonating frequency of 2.45 GHz. Miniaturization is attained through etching four open-end slots on the rectangular patch along the  $x$ -axis on both the sides. L-shaped partial ground plane is used for better impedance matching and wider bandwidth. Length of the slots and other parameters are optimized to tune the desired resonance using Computer Simulation Technology (CST) microwave studio.

As the antenna is designed to be operated on the human body, all the simulations and optimization during design process performed on the three-layered tissue model consist of skin ( $\epsilon_r = 38$  and  $\sigma = 1.46 \text{ s/m}$ ), fat ( $\epsilon_r = 5.2$  and  $\sigma = 0.10 \text{ s/m}$ ), and muscle ( $\epsilon_r = 52.7$  and  $\sigma = 1.8 \text{ s/m}$ ). The planar dimension of tissue modal is  $40 \times 60 \text{ mm}^2$  and its properties are taken according to [20, 21]. The geometrical structure of single-element antenna along with on-body simulation setup and surface current distribution is shown in Fig. 1.

### Stepwise evaluation of single radiator antenna

Stepwise design evaluation of antenna is represented in Fig. 2. Comparison of reflection coefficient  $S_{11}$  for all the design steps is shown in Fig. 3. The proposed structure is initially designed as a rectangular microstrip patch with the partial ground plane. By etching multiple open-end slots, this structure is modified to resonance at a desired 2.45 GHz frequency.

In step 1, the antenna is designed by cutting two open-end slots at the two opposite corners of the radiator. First slot is etched at the lower left corner which provides wideband

resonance at 3.5 GHz. Length CW1 of the slot is varied from 8 to 11 mm to obtain optimal performance. From Fig. 4(a), it can be observed that increasing the length of the slot helps to reduce the resonating band but degrades impedance matching. Therefore, CW1 = 9 mm is considered for further design which provides resonance at 3.9 GHz. Second slot is etched at the upper right corner which adds inductive effect in the structure. It helps to reduce the resonating band from 3.9 to 3.0 GHz with good impedance matching. Effect of varying length CW4 is shown in Fig. 4(b). The increasing value of CW4 has an almost negligible effect on return loss.

In step 2, a new slot parallel to the first slot is etched that induces the inductive effect and shift the antenna resonance at 2.8 GHz. Impedance plot for the evaluation steps of the antenna is shown in Fig. 5. In step 2, reactance shifts upward which shows high inductive reactance ( $x_l = \omega l$ ) in impedance. The high value of inductance helps to lower the resonance from 3 to 2.8 GHz. The optimal value of this slot is taken as “CW2 = 7 mm” for the design.

Further in step 3 (Fig. 2(c)), another slot is etched parallel to the top right slot to achieve the resonance at 2.45 GHz. Reactance plot shifts downward making impedance more capacitive ( $x_c = 1/\omega c$ ). From Fig. 3, it can be found that a reflection coefficient of 20 dB and a bandwidth of 120 MHz are obtained in step 3. It is well known that the human body is a complex structure with multiple tissue layers. The thickness and electric properties of tissue layers vary for different body parts as well as for the individual. It was studied in the present literature that antenna frequency may detune and impedance matching degrades when subjected to various parts of the body [9, 12, 22, 23]. Thus, to overcome the limitation of frequency detuning and impedance

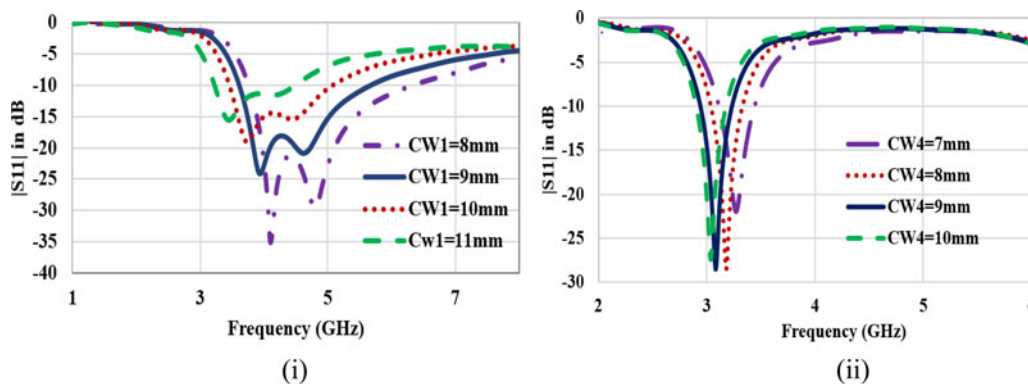


Fig. 4. Effect of varying slot lengths on reflection coefficient in step 1: (a) varying  $CW1$  and (b) varying  $CW4$ .

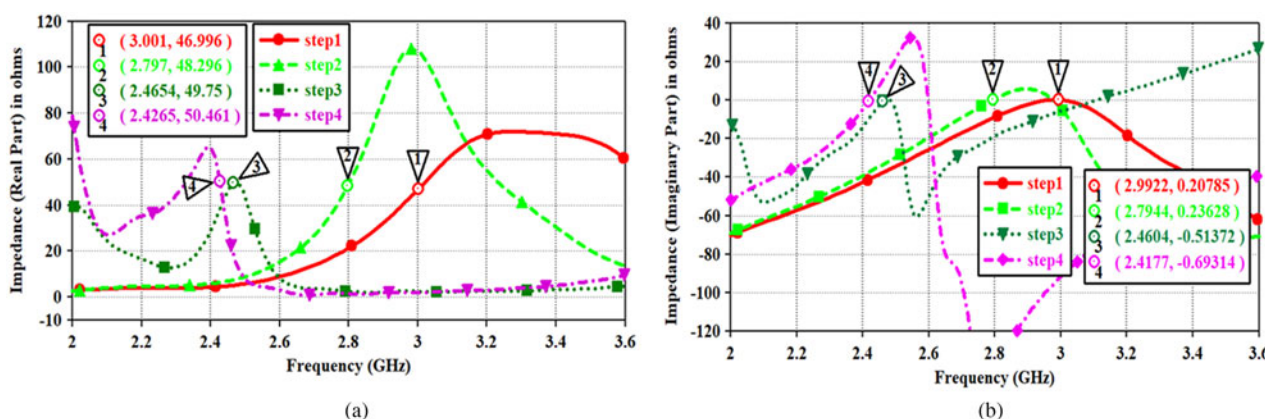


Fig. 5. Plot for input impedance: (a) real part and (b) imaginary part.

mismatch in practical applications, the structure is modified by using defected ground structure in step 4.

Partial ground plane is converted into an L-shaped ground plane. It tends to reduce the quality factor ( $Q$ ) and improve the bandwidth ( $BW$ ) of the proposed structure ( $BW = Fr/Q$ ). Impedance curve represents 50 ohm resistance and null reactance at 2.42 GHz. Reactance curve is shifting upward showing an increase in inductance value and reduction in  $Q$ -factor. Significant improvement in reflection coefficient from 13 to 40 dB and a bandwidth of 300 MHz is obtained without altering the central resonating frequency.

To analyze the working principle, a relationship among slot dimensions and the resonance frequency is established. Surface current distribution in Fig. 1(d) shows the resonating path at 2.45 GHz. Surface current has followed the meandered path through the open-end slots. Therefore, the length of the radiating path ( $LR$ ) responsible for resonance can be calculated as

$$LR = \frac{(WP - WF)}{2} + D1 + (2 \times CW1) + D2 + (2 \times CW2) + D3. \tag{1}$$

From Fig. 1 and data given in Table 1,  $LR = 47.3$  mm. Here, the effective dielectric constant ( $E_{eff}$ ) is calculated as 1.645.  $LR$  should be half wavelength at the resonance; therefore, resonating

Table 1. Geometrical parameters of the proposed structure

Parameter	Value (mm)	Parameter	Value (mm)
W	14	L	25
D1	4.53	CW1	4.47
D2	4.41	CW2	7.34
D3	9.26	CW3	9.3
D4	3.9	CW4	8.85
D5	7.18	WP	13
LF	4.8	WF	2
LG	3.2	WG	13.0
Lc	13.5	Wc	20.0
WS	2.0	LS	4.4

frequency  $f_{r1}$  at this length is

$$f_{r1} = \frac{c}{2 \times LR \times \sqrt{E_{eff}}} \approx 2.477 \text{ GHz}. \tag{2}$$

It shows that the calculated frequency from the antenna design parameters is in good agreement with the desired frequency.



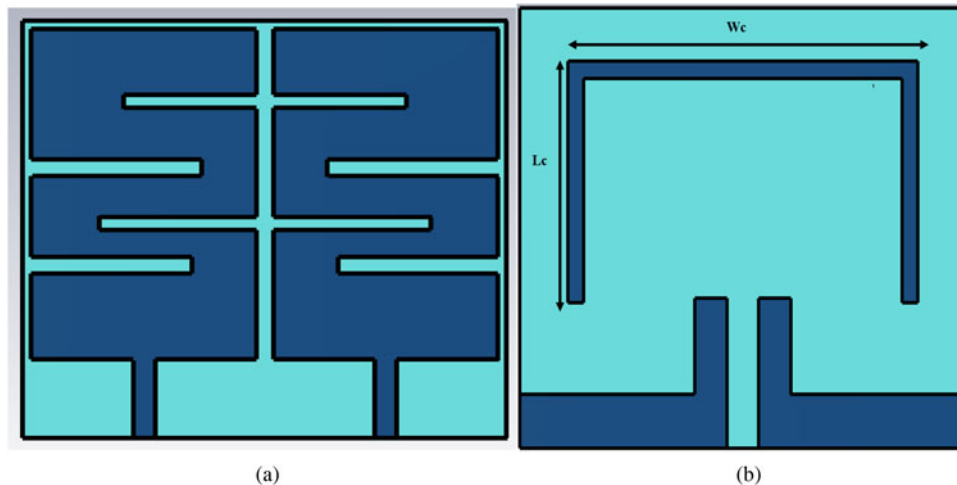


Fig. 6. Structure of MIMO antenna: (a) front view and (b) back view.

### Design of MIMO structure

To design a MIMO antenna, two mirror image antenna elements are placed parallel to each other. It was difficult to maintain high isolation between two elements without a decoupling structure. Therefore, to improve the isolation, inverted U-shaped stub is added at the ground plane acting as a parasitic resonator. Length of this stub is 47 mm ( $2 \times L_c + W_c$ ), which is approximately equal to the value calculated in equation (1). Length of inverted U-shaped stub satisfies the resonating length at 2.45 GHz. The geometry of the MIMO structure is shown in Fig. 6. S-parameters of the antenna with and without ground stub are compared in Fig. 7. Adding of stub has enhanced the isolation from 11 to 32 dB.

The design approach for adding inverted U-shaped stub can be explained with the help of the surface current shown in Fig. 8. It can be observed that the current is excited from the open edge of the lowermost slot and the maximum current is followed through the slots. Therefore, decoupling stub is added from the current excitation point of radiator 1 to radiator 2. From the surface current plot (Figs 8(b) and 8(c)), it can be found that the current flowing from port 1 to port 2 is offset by the ground stub which reduces mutual coupling between antenna elements.

### Effect of varying separation gap “s” between antenna and body tissue on antenna performance

The large variation in the permittivity of body tissue and antenna substrate causes varying effective dielectric constant of the antenna which significantly detunes the resonating band. Therefore, the antenna is placed at a gap “s” from the tissue model to avoid degradation of antenna performance. Human body keeps on moving, it is hard to maintain the constant separation gap all the time. For this reason, three different values of gap ( $s = 2, 4, 6$  mm) are used to account the border of antenna reliability. Reflection coefficient, radiation efficiency, and gain plot for varying “s” are shown in Fig. 9.

Reducing the value of “s” causes lowering of central resonating frequency. From Fig. 8(a), it can be observed that due to wide bandwidth, the proposed structure can effectively cover the desired ISM band from 2.4 to 2.48 GHz for all values of s. At “s = 4 mm”, a resonating frequency of 2.45 GHz is obtained. Therefore, for all, the simulation and measurement value of “s” is kept at 4 mm.

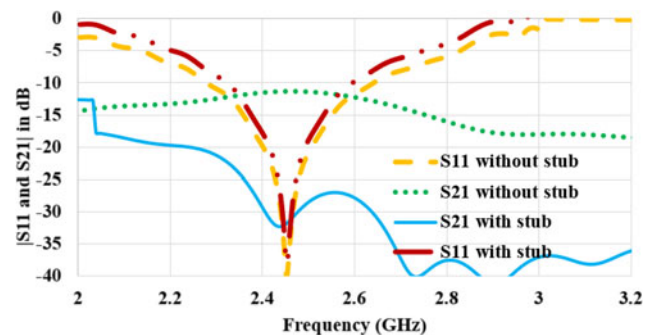


Fig. 7. S-parameters of MIMO antenna with and without stub.

Antenna shows the lowest gain of  $-0.9$  dB and an efficiency of 38% when placed in extreme proximity ( $s = 2$  mm) of body tissue. Some of the near-field power is absorbed ( $P_{abs}$ ) by the tissue. It depends upon the conductivity ( $\sigma$ ) of tissue layers and near-field electric field intensity ( $E$ ) [2]. Electrical field intensity in the near field is given in equation (4), which shows field intensity reduces with increasing distance from the antenna [24]. Therefore, an improvement in the gain of 1.2 dB and in the efficiency of 8% is observed with increasing s from 2 to 6 mm.

$$P_{abs} = \frac{1}{2} \sigma |E^2| dV, \quad (3)$$

$$E = \frac{I_m \times LR \times \sin \theta}{4\pi\epsilon} \left[ \frac{-\omega \sin \omega t}{c^2 s} + \frac{\cos \omega t}{s^2 c} + \frac{-\omega \sin \omega t}{s^3 \omega} \right]. \quad (4)$$

### Results and discussion

The proposed antenna is fabricated to validate the simulated results. Antenna parameters are measured using Agilent N5247A programmable network analyzer and anechoic chamber. The actual on-body performance of the fabricated antenna is measured on a pork loin. Photographs of the experimental setup are shown in Fig. 10.

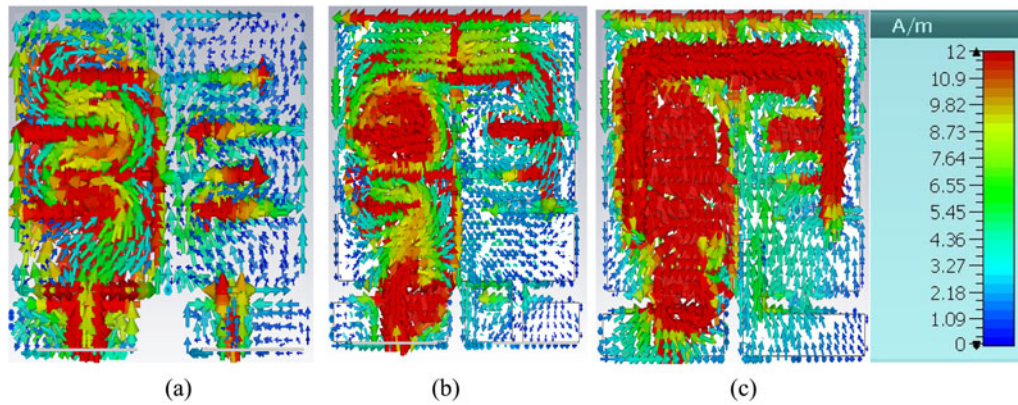


Fig. 8. Surface current distribution of MIMO antenna (a) without stub, (b) with stub front view, and (c) back view.

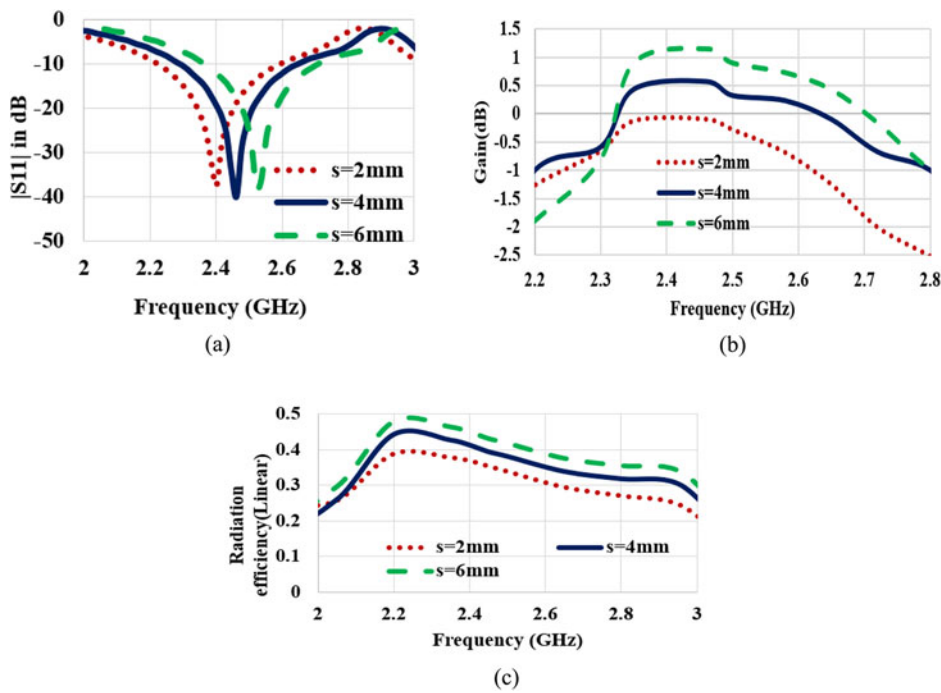


Fig. 9. Effect of varying “s” on antenna performance: (a) reflection coefficient, (b) gain, and (c) radiation efficiency.

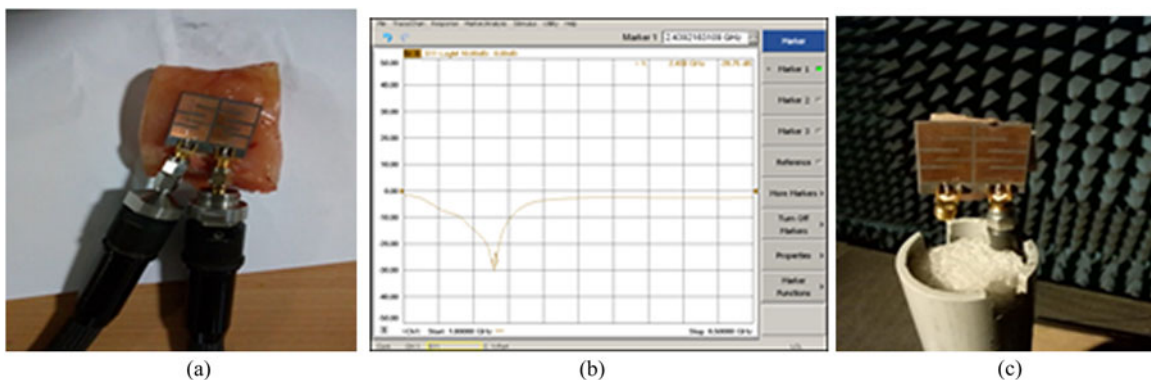


Fig. 10. Photographs of the experimental setup: (a) antenna placed on pork loin, (b) return loss plot on VNA, and (c) antenna in an anechoic chamber.

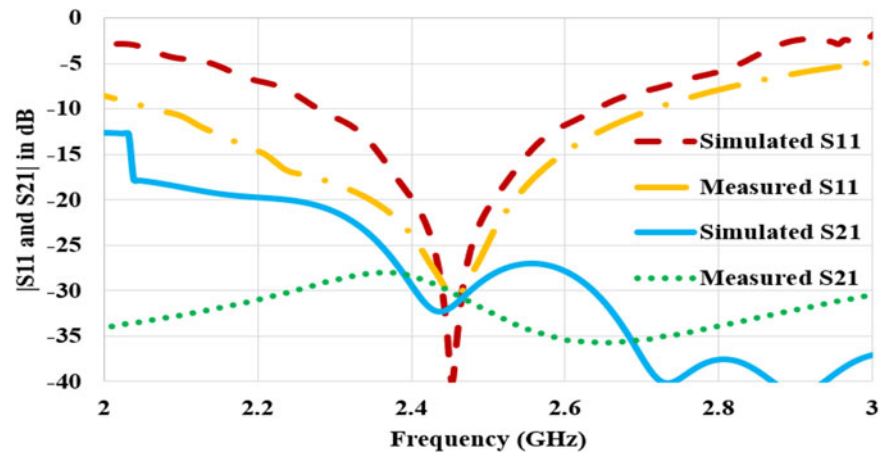


Fig. 11. Measured and simulated reflection coefficient.

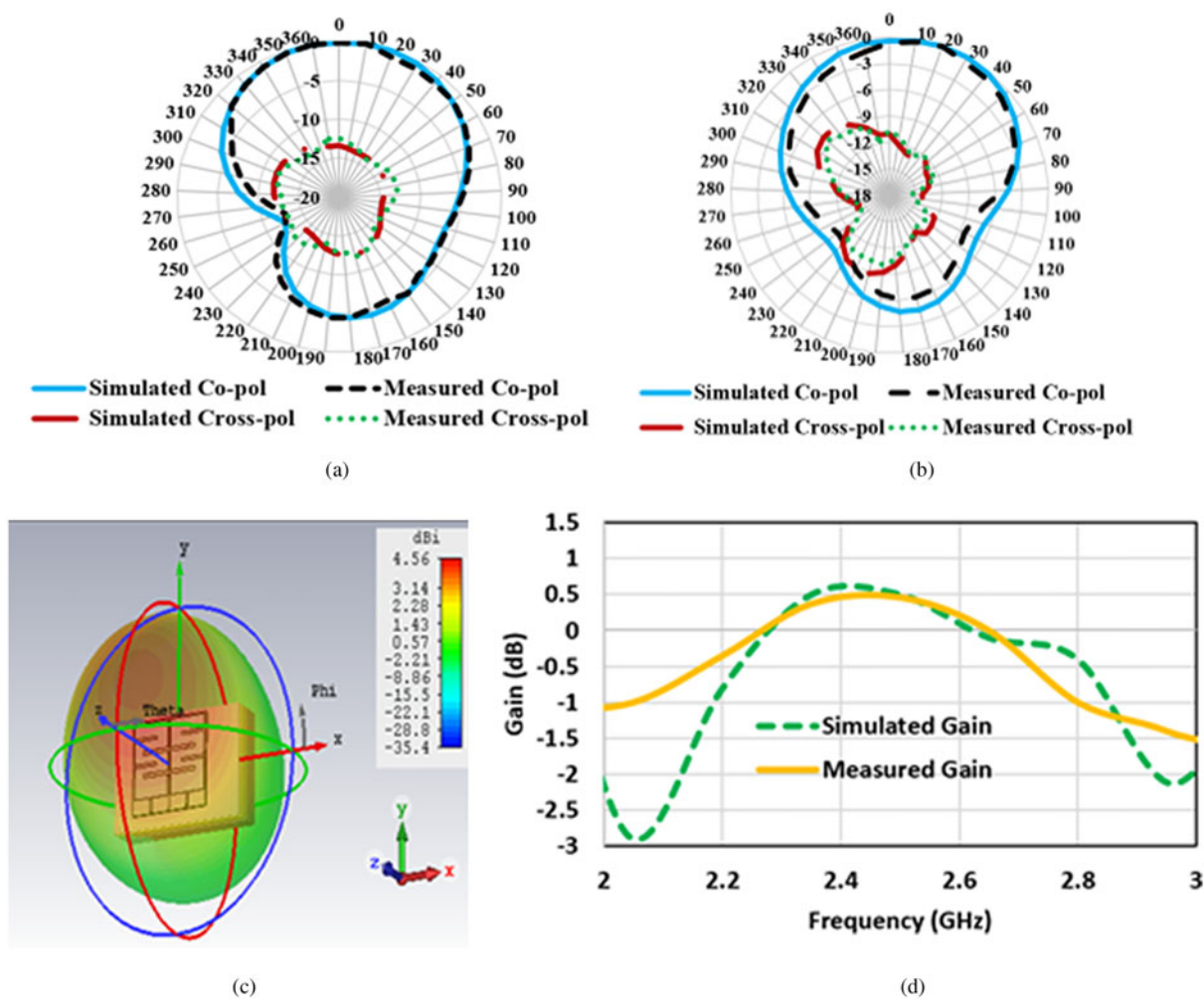


Fig. 12. (a) E-plane radiation pattern, (b) H-plane radiation pattern, (c) simulated 3D radiation pattern at 2.45 GHz, and (d) plot for simulated and measured gain over the frequency.

### S-parameters

Scattering parameters are measured to analyze the impedance matching and level of mutual coupling in terms of reflection coefficient ( $S_{11}$ ) and transmission coefficients ( $S_{21}$ ), respectively. Plot for simulated and measured S-parameters is shown in Fig. 11.

Simulated 10 dB bandwidth is 300 MHz (2.3–2.6 GHz) whereas measured bandwidth is 480 MHz (2.12–2.6 GHz). Measured data reveal wider bandwidth as compared to the simulation data. A similar type of variation in simulated and measured results has been observed in [6, 13, 25]. Simulated and measured



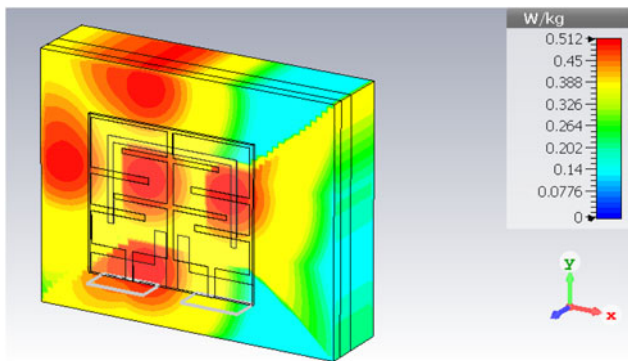


Fig. 13. SAR value of the proposed MIMO antenna.

transmission coefficient shows that mutual coupling is less than  $-30$  dB for the required ISM band.

**Radiation characteristics**

Simulated and measured E-plane and H-plane radiation patterns for excitation at port 1 are shown in Figs 12(a) and 12(b). It can be seen that broadside radiation pattern toward  $+z$  direction is

offered by the antenna which is the required feature for the on-body antenna. Three-dimensional plot for directivity at 2.45 GHz is shown in Fig. 12(c). Maximum directivity of 4.56 dBi is obtained. Power is radiated away from the body. Each layer of body tissue has different permittivity and thickness which causes the internal reflection of electromagnetic waves. Therefore, superposition of antenna back radiation and reflections from the multi-layered human tissue introduces an improvement of directivity. The simulated and measured gain plot is shown in Fig. 12(d). It shows that antenna retains positive gain for the operating bandwidth.

**Specific absorption rate**

Near-field radiations of the wearable antenna affect the human body. Continuous exposure of radiations increases the temperature of the tissue. Heat is generated due to the non-radiating reactive near field. Excessive heat may damage cells and reduces the blood circulation causing a disturbance in the functioning of sensitive organs. Thus, it is necessary to consider the power absorbed by body tissue. Standard measure to evaluate this absorbed electromagnetic power by the body is defined as the specific absorption rate.

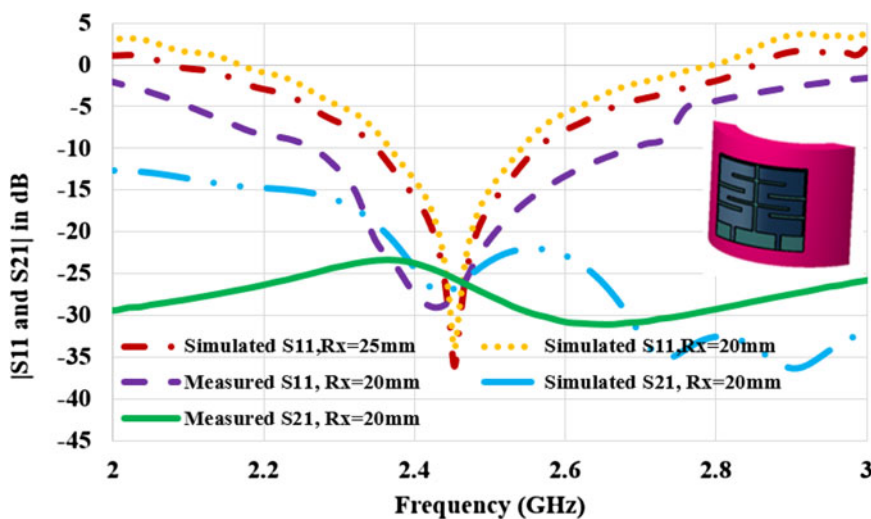


Fig. 14. S-parameters for bending along the x-axis.

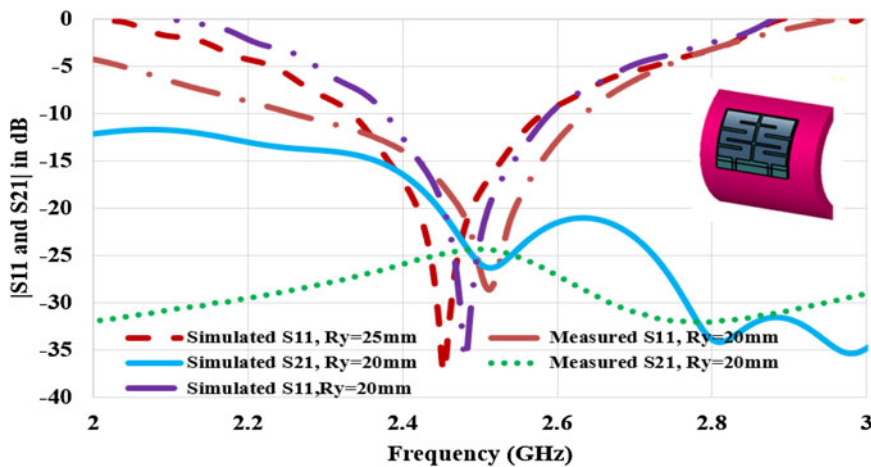


Fig. 15. S-parameters for bending along the y-axis.



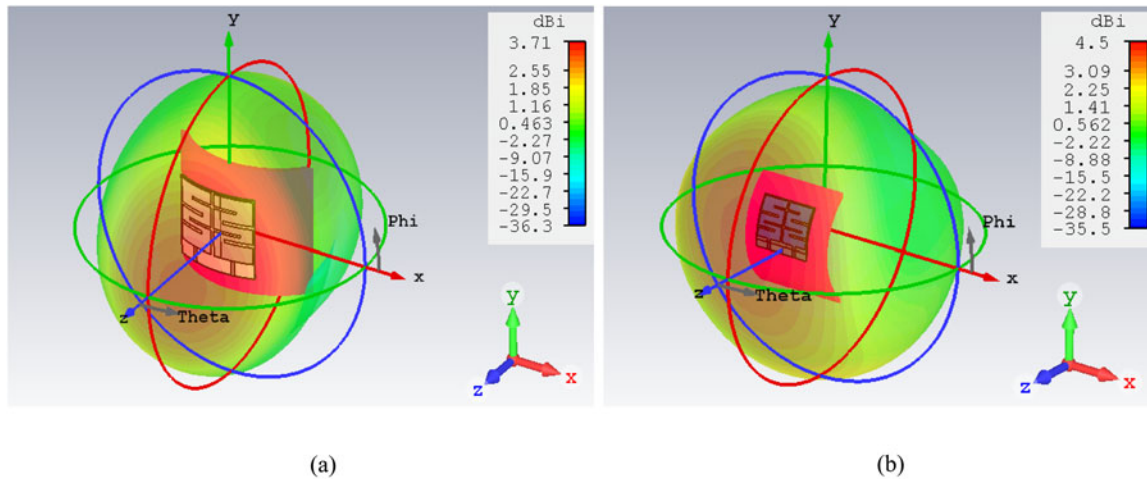


Fig. 16. 3D radiation plot for deformation cases: (a) along the  $x$ -axis and (b) along the  $y$ -axis.

According to the IEEE C95.1-2005 standard, SAR value should not be larger than 2 W/Kg averaged over 10 g of tissue in the shape of a cube [26]. Simulated SAR for the proposed antenna at 2.45 GHz is shown in Fig. 13. The antenna has the maximum SAR value of 0.512 W/Kg for 0.1 W of input power. The obtained value is well below the maximum safety limit.

#### Effect of bending on antenna performance

In WBAN, wearable antennas are supposed to bend during various body movements. Therefore, antenna performance is examined under structural deformation. The antenna is bent across a circular phantom with two different radii of values 25 and 20 mm. Radii are considered according to the average wrist size of adults. For the larger radii, the antenna is self-conformal due to its compact size. Variable  $R_x$  and  $R_y$  are taken to represent the bending radii along the  $x$ - and  $y$ -axis, respectively. Reflection coefficient ( $S_{11}$ ) for all the radii and transmission coefficient ( $S_{21}$ ) for extreme bending are shown in Fig. 14 ( $x$ -axis bending) and in Fig. 15 ( $y$ -axis bending).

In the case of  $x$ -axis bending, a negligible effect on resonating frequency and impedance matching is observed with decreasing radii. Due to extreme bending at 20 mm, simulated reflection coefficient shifts from  $-40$  to  $-34$  dB when compared with a flat structure. Measured result for bending across  $R_x = 20$  mm also shows stable performance. Mutual coupling is not affected by the structural deformation along the  $x$ -axis.

In the case of  $y$ -axis bending, a slight frequency detuning of frequency toward rightward is obtained with reducing radii. The simulated reflection coefficient is degraded from  $-40$  to  $-35$  dB at the radii of 20 mm as compared to a flat structure. This effect is due to the variation in the gap between open-end slots and their width. Measured reflection coefficient shows the significant shifting of central resonating frequency from 2.45 to 2.51 GHz. Still, the antenna can effectively cover the ISM band due to its wide-band performance. Mutual coupling is also affected with  $y$ -axis deformation. Bent along  $y$ -axis has stretched the length of vertical arms of the ground stub. This probably degrades the isolation. It can be also observed that smaller radius has stronger bending effects on antenna performance. Simulated and measured results show that the proposed structure can maintain the reflection

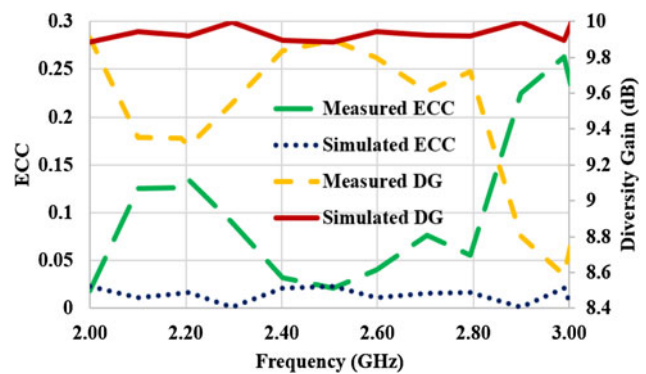


Fig. 17. ECC and DG of the proposed antenna.

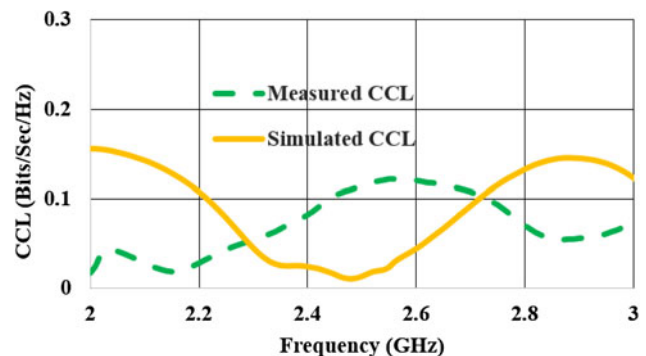


Fig. 18. Plot for channel capacity loss (CCL).

coefficient for the ISM band well below  $-10$  dB for all the bending radii of  $R_x$  and  $R_y$ .

Three-dimensional radiation plot for the bending condition is shown in Fig. 16. For both the deformation conditions, maximum radiation is oriented away from the body tissue. For the  $x$ -axis bending, reduction in directivity is observed as compared to a flat structure. Stable response for radiation pattern is established while bending along the  $y$ -axis.

**Table 2.** Comparison of the proposed antenna with the existing on-body antennas

Ref.	Frequency (GHz)	Material used	Size (mm <sup>3</sup> )	Gain (dBi)	Bandwidth (MHz)	Efficiency (%)	SAR (W/Kg.) with input power	Port isolation (dB)
[3]	2.45	Textile foam, $\epsilon_r = 1.45$	65.6 × 58.9 × 3.9	6.5	337	73	NA	NA
[5]	2.4/5.5	Butadiene rubber fabric (NBR-F) $\epsilon_r = 2.9$	50 × 40 × 4.6	NA	500/1000	25/27	0.428/1.87 at 100 mW	NA
[9]	2.45	Felt, $\epsilon_r = 1.2$	$r = 24$ mm, $h = 1$ mm	-12.03	170	14	0.4 at W	NA
[10]	2.45	FB4, $\epsilon_r = 2.55$	$r = 24$ mm, $h = 3.2$ mm	-3.03	83	NA	5.04 at 1 W	NA
[13]	2.45	Felt, $\epsilon_r = 1.2$	46 × 25 × 2	0.64 dB	105	NA	NA	NA
[14]	2.45, 5	Felt, $\epsilon_r = 1.3$	101.9 × 92.3 × 3	NA	160/671	50/58	0.056/0.067 at 0.5 W	20
[15]	UWB (2.74–12)	Jeans, $\epsilon_r = 1.6$	110 × 35 × 1.5	6.9 dB	9.26 GHz	NA	NA	26
[16]	UWB (3.5–8)	Jeans, $\epsilon_r = 1.6$	30 × 50 × 1.5	NA	700	NA	NA	32
[17]	2.45	Fr-4, $\epsilon_r = 4.4$	30 × 30 × 0.5	NA	140	40	NA	20
[18]	2.45	Fr-4, $\epsilon_r = 4.4$	Radius = 22.9 mm, $h = 3.2$ mm	3	90	40	0.55 at 100 mW	15
[19]	2.45	Fr-4, $\epsilon_r = 4.4$	54.98 × 76 mm <sup>2</sup>	2.83	1900	NA	1.2	12
Proposed work	2.45	Rogers 5880, $\epsilon_r = 2.2$	28 × 25 × 0.5	0.5 dB	300	40	0.512 for 0.1 W	30

**Diversity performance**

To support the MIMO capability of the proposed antenna, important diversity parameters envelope correlation coefficient (ECC), diversity gain (DG), and channel capacity loss (CCL) are analyzed as explained in [16, 18]. ECC signifies the correlation of antenna radiation pattern with another antenna when operated in closed proximity. The high value of ECC degrades the antenna MIMO performance. ECC value lower than 0.5 is acceptable for MIMO antennas. ECC is calculated using the 3D radiation pattern as

$$\rho_e = \frac{|\iint_{\Omega} \vec{E}_1(\theta, \phi) \cdot \vec{E}_2^*(\theta, \phi) d\Omega|^2}{\iint_{\Omega} |\vec{E}_1(\theta, \phi)|^2 d\Omega \cdot \iint_{\Omega} |\vec{E}_2(\theta, \phi)|^2 d\Omega}, \tag{5}$$

where  $\vec{E}_1(\theta, \phi)$  and  $\vec{E}_2^*(\theta, \phi)$  are the far fields of antenna for radiator 1 and radiator 2.

DG shows the accomplishment of diversity performance of MIMO antenna and it can be evaluated using ECC.

$$DG = 10\sqrt{(1 - |\rho_e|)}. \tag{6}$$

Simulated and measured ECC and DG plots are shown in Fig. 17. It can be observed that ECC results are well below 0.025 and DG is more than 9.8 dB for 2.4–2.48 GHz.

CCL limits the data transmission rate over the channel. The low value of CCL ensures higher data rate. The value of CCL should be <0.4 bits/s/Hz for a MIMO system. CCL can be evaluated as

$$CCL = -\log_2 \det(a^R), \tag{7}$$

where  $a^R$  is the 2 × 2 correlation matrix and its elements are given as  $a_{ii} = 1 - (|S_{ii}|^2 + |S_{ij}|^2)$ ;  $a_{ij} = 1 - (S_{ii}^* S_{ij} + S_{ij}^* S_{ii})$ .

Measured and simulated CCL are shown in Fig. 18. The proposed structure has <0.12 bits/s/Hz value of CCL at ISM band.

**Conclusion**

We have demonstrated a MIMO antenna structure for on-body communication. A prototype covering 2.45 GHz band is designed, fabricated, and its performance is measured on pork loin. The proposed MIMO structure has an overall dimension of 28 × 25 × 0.51 mm<sup>3</sup>. The wide bandwidth of 300 MHz is suitable to maintain a robust communication link when operated in a different biological environment. Improved port isolation of 30 dB and a good diversity performance are obtained. Stable performance is obtained when the antenna is subjected to structural deformation. Low SAR value of 0.512 W/Kg ensures the user’s safety. Antenna performance is compared with the existing single-element and MIMO-based on-body antennas in Table 2. The proposed structure is the smallest of all the antennas compared in Table 2 with satisfactory on-body as well as diversity performance.

**References**

1. **Chen M, Gonzalez S, Vasilakos A, Cao H and Leung VC** (2011) Body area networks: a survey. *Mobile Networks and Applications* **16**, 171–193.
2. **Kiourti A and Nikita KS** (2012) A review of implantable patch antennas for biomedical telemetry: challenges and solutions. *IEEE Antennas and Propagation Magazine* **54**, 210–227.

3. **Moro R, Agneessens S, Rogier H and Bozzi M** (2018) Circularly-polarised cavity-backed wearable antenna in SIW technology. *IET Microwaves, Antennas & Propagation* **12**, 127–131.
4. **Agneessens S** (2017) Coupled eighth-mode substrate integrated waveguide antenna: small and wideband with high-body antenna isolation. *IEEE Access* **6**, 1595–1602.
5. **Al-Schemi A, Al-Ghamdi A, Dishovsky N, Atanasov N and Atanasova G** (2018) Design and performance analysis of dual-band wearable compact low-profile antenna for body-centric wireless communication. *International Journal of Microwave and Wireless Technologies* **10**, 1–11.
6. **Gao GP, Hu B, Wang SF and Yang C** (2018) Wearable circular ring slot antenna with EBG structure for wireless body area network. *IEEE Antennas and Wireless Propagation Letters* **17**, 434–437.
7. **Alemaryeen A and Noghianian S** (2017) Crumpling effects and specific absorption rates of flexible AMC integrated antennas. *IET Microwaves, Antennas & Propagation* **12**, 627–635.
8. **Lilja J, Salonen P, Kaija T and Maagt P** (2012) Design and manufacturing of robust textile antennas for harsh environments. *IEEE Transactions on Antennas and Propagation* **60**, 4130–4140.
9. **Tak J, Lee S and Choi J** (2014) All-textile higher order mode circular patch antenna for on-body to on-body communications. *IET Microwaves, Antennas & Propagation* **9**, 576–584.
10. **Tong X, Liu C, Liu X, Guo H and Yang X** (2018) Switchable on-/off-body antenna for 2.45 GHz WBAN applications. *IEEE Transactions on Antennas and Propagation* **66**, 967–971.
11. **Lin CH, Saito K, Takahashi M and Ito K** (2012) A compact planar inverted-F antenna for 2.45 GHz on-body communications. *IEEE Transactions on Antennas and Propagation* **60**, 4422–4426.
12. **Shakib MN, Moghavvem M and Mahadi WN** (2017) Design of a tri-band off-body antenna for WBAN communication. *IEEE Antennas and Wireless Propagation Letters* **16**, 210–213.
13. **Hu B, Gao GP, He LL, Cong XD and Zhao JN** (2017) Bending and on-arm effects on a wearable antenna for 2.45 GHz body area network. *IEEE Antennas and Wireless Propagation Letters* **15**, 378–381.
14. **Yan S, Soh PJ and Vandenbosch GAE** (2015) Dual-band textile MIMO antenna based on substrate integrated waveguide (SIW) technology. *IEEE Transactions on Antennas and Propagation* **63**, 4640–4647.
15. **Biswas AK and Chakraborty U** (2019) Compact wearable MIMO antenna with improved port isolation for ultra-wideband applications. *IET Microwaves, Antennas & Propagation* **13**, 498–504.
16. **Biswas AK and Chakraborty U** (2019) Investigation on decoupling of wideband wearable multiple-input multiple output antenna elements using microstrip neutralization line. *RF and Microwave Computer Aided Engineering* **e21723**, 1–11.
17. **Qu L, Piao H, Qu Y, Kim H and Kim H** (2018) Circularly polarised MIMO ground radiation antennas for wearable devices. *IET Electronics Letters* **54**, 189–190.
18. **Dingliang W, Yang H, Max OM and Hanyang WHZ** (2018) A compact and low-profile MIMO antenna using a miniature circular high-impedance surface for wearable applications. *IEEE Transactions on Antennas and Propagation* **66.1**, 96–104.
19. **Chouhan S, Panda DK, Khushwah PK and Mishra PK** (2019) Octagonal-shaped wideband MIMO antenna for human interface device and S-band application. *International Journal of Microwave and Wireless Technologies* **11**, 287–296.
20. **Gemio J, Parron J and Soler J** (2010) Human body effects on implantable antennas for ISM band applications: models comparison and propagation losses study. *Progress in Electromagnetic Research* **110**, 437–452.
21. **Chen Z, Gao YM and Du M** (2018) Propagation characteristics of electromagnetic wave on multiple tissue interfaces in wireless deep implant communication. *IET Microwaves, Antennas & Propagation* **12**, 2034–2040.
22. **Abbasi MB, Nikolaou S, Antoniadis M, Stevanovic MN and Vryonides P** (2017) Compact EBG-backed planar monopole for BAN wearable applications. *IEEE Transactions on Antennas and Propagation* **65**, 453–462.
23. **Duan Z, Xu L and Geyi W** (2017) Metal frame repeater antenna with partial slotted ground for bandwidth enhancement of wristband devices. *IET Microwave Antennas Propagation* **11**, 1438–1444.
24. **Prasad KD and Handa D** (2003) *Antenna and Wave Propagation*, 3rd Edn. New Delhi, India: Satya Parkashan.
25. **Koo T, Hong Y, Park G, Shin K and Yook J** (2015) Extremely low-profile antenna for attachable bio-sensors. *IEEE Transactions on Antennas and Propagation* **63**, 1537–1544.
26. **IEEE Std. C95.1** (2005) IEEE standard for safety levels with respect to human exposure to the radio frequency electromagnetic fields 3 kHz to 300 GHz.



etry, and electromagnetics.

**Anupma Gupta** received her B.Tech degree in Electronics and Communication Engineering from Guru Jambheshwar University, India, in 2006 and M.Tech degree from Maharishi Markandeshwar University, Mullana, India, in 2010. She is currently working toward the Ph.D. degree at Thapar University. Her main research interests are the design and optimization of microstrip antennas, biomedical telem-



conference. He is a lifetime member of ISTE. His research interests include net-

**Ankush Kansal** received his B.Tech. and M.Tech. degree in Electronics and Communication Engineering from PTU, Jalandhar and the Ph.D. degree from Thapar University, Patiala in the area of Wireless Communication. He is currently working as an Assistant Professor at Thapar University, Patiala. He has published 25 research articles in referred international journals, international conference, and national



working, wireless communication, image processing, and embedded systems.

**Paras Chawla** received his B.Tech (Honors) and M.Tech degree in Electronics and Communication Engineering from Kurukshetra University, NIT, Kurukshetra and the Ph.D. degree from Thapar University, Patiala. He has more than 14 years of teaching experience and currently working as a Professor and HOD in the ECE Department at Chandigarh University, Mohali (India). He guided a total of 16 M.Tech dissertations successfully and also guiding seven students of the Ph.D. degree. He received the “Coventor Scholarship award” from MANCEF, New Mexico, USA for his proposal in the conference COMS-2010. His team received consecutively 2 years the “Tenderfoot Award” collaboratively given by American Astronautical Society and American Institute of Aeronautics, for “CanSat Competition”, June 2015 and 2016, Burkett, Texas, USA. His main research interests include microstrip antennas, RF MEMS, RF front-end mobile terminal, LTE, and 5G. He has published more than 50 papers in various reputed national and international journals/conferences, one SCI book chapter, and 10 patents filed.